A DIAGNOSTIC STUDY ON SEASONAL VARIATIONS OF STRATOSPHERIC DIABATIC CIRCULATION AND ASSOCIATED OZONE TRANSPORT

by

Pi-Huan Wang

Science and Technology Corporation, Hampton, Virginia 23666

A. Ghazi[1]

Commission of the European Communities, 1049 Brussels, Belgium

M. P. McCormick

Atmospheric Sciences Division, NASA-Langley Research Center, Hampton, Virginia

(NASA-CR-185309) A DIAGNOSTIC STUDY ON SEASONAL VARIATIONS OF STRATOSPHERIC DIABATIC CIRCULATION AND ASSOCIATED OZCNE TRANSPORT (NASA. Langley Research Center) 61 p

N89-71112

Unclas
00/46 0213162

---

1. Privatdozent, University of Cologne, FRG

ABSTRACT

In this paper, the authors present the results of a diagnostic study on seasonal variations of the stratospheric diabatic circulation in isentropic coordinates. The data sets used in the analysis comprised the entire 34-month ozone observations (February 1979 - November 1981) of the Stratospheric Aerosol and Gas Experiment (SAGE) and the associated temperature profiles provided by NOAA. In addition, the seasonal variations of the corresponding transport effect of this circulation on ozone distribution are also examined.

The results indicate that in the lower stratosphere, the derived diabatic circulation exhibits basically a two-cell mass flow pattern during both equinox and solstice. In comparison, the circulation in the upper stratosphere shows mainly a single cell pattern during solstice and a two-cell structure during equinox. Similarly, the calculated flux divergence of the air mass weighted ozone concentration associated with the derived diabatic circulation shows differences in the seasonal variations between the lower and the upper stratosphere. The essentially year-round two-cell pattern of the calculated diabatic circulation in the lower stratosphere provides a qualitative

explanation for the observed persistent convex structure of ozone distribution in this region.

1. Introduction

The objective of this study is to examine seasonal variations of the stratospheric diabatic circulation and the associated ozone transport utilizing the ozone data sets from the Stratospheric Aerosol and Gas Experiment (SAGE) observations for its entire 34-month lifetime (February 1979-November 1981). The ozone measurements from the SAGE satellite instrument, together with the corresponding meteorological information from NOAA (temperatures and heights at 18 standard pressure levels at the time and location of the SAGE measurement events), provide a unique opportunity for such an investigation.

It is well known that the stratosphere is controlled by strongly coupled processes involving radiation, photochemistry, and dynamics (e.g., Hartmann, 1981; Brasseur and Solomon, 1984). The atmospheric trace constituents that determine the distribution of the net thermal energy through radiative absorption and emission processes, and in turn determine the circulation system, are themselves influenced by the transport effect of the circulation. In an earlier analysis of middle atmospheric circulation, efforts involved the determination of a meridional circulation for a calculated distribution of

differential net zonal mean radiative heating, corresponding to a particular season (Murgatroyd and Singleton, 1961; Leovy, 1964; Holton, 1975). In this regard perhaps, the thermal energy which arises from absorption of incoming solar radiation by minor atmospheric constituents, mainly ozone, can be approximately regarded as a forcing mechanism of the middle atmospheric circulation, and the corresponding thermal and chemical structures can be regarded as manifestations of the middle atmosphere in response to this forcing. With this in mind, it is clear that there are two essential components of such forcing corresponding to two different time scales acting in the middle atmosphere; namely, the forcing with time scales of a season, and a day. More specifically, they are variations associated with the changes in the earth-sun geometry. The seasonal time scale is associated with variations of the sun declination and the daily scale of the earth's rotation. The atmospheric response to the latter forcing is related to the well-known phenomenon--the atmospheric tide (Chapman and Lindzen, 1970). The response to the former has been interpreted as the diabatic circulation (Dunkerton, 1978; Holton, 1981; Holton and Wehrbein, 1980, etc.). In this study, the analysis is focused on the dynamics system of seasonal variations utilizing recent satellite

observations in the stratosphere.

It has been recognized that the stratospheric circulation and the distribution of the minor stratospheric constituents exhibit sustained large gradients in latitude with relatively mild gradients in longitude, except at northern high latitudes during late winter and early spring. This prevailing characteristic suggests that the stratospheric circulation can be described appropriately by an averaged mean component plus a departure (the planetary waves) from the average--a two-dimensional analysis. It has also been recognized that this mean component is largely characterized by seasonal variations and corresponds mainly to the diabatic circulation (Murgatroyd and Singleton, 1961; Leovy, 1964; Holton and Wehrbein, 1980). The departure has been shown to be closely related to the large-scale meteorological disturbances in the troposphere (Charney and Drazin, 1961; Matsuno, 1971; Holton, 1976; Quiroz, 1979; Dickinson, 1980; Schoeberl and Strobel, 1980).

The understanding of the nature of stratospheric diabatic circulation and its counterpart, i.e., the wave dynamics, has undergone interesting development during the last half century. Evidence has determined that the mathematically derived behavior

of both the mean middle atmospheric circulation and the departure system depend on specific averaging procedures used in the analysis (e.g., the extensive review article by Mahlman et al., 1984). Furthermore, it is well-known that the conventional approach in which the zonal average is derived along a constant latitude on a given height or pressure surface, the so-called Eulerian formulation, leads to a thermally indirect meridional circulation featured by upward motions in the winter polar region and over the tropics and descending motions over the middle latitudes. This situation is opposed to the so-called Brewer-Dobson circulation in which tracer transport takes place by rising motions through the tropical tropopause and sinking motions in the winter high latitudes, as argued by Brewer (1949) and Dobson (1956) based on observed water vapor and ozone distributions. The difficulty of Eulerian mean circulation in describing the tracer distribution lies in the fact that the net transport is a small residue between the transports associated with the Eulerian mean circulation and the departure field from the mean (Hunt and Manabe, 1968; Mahlman, 1969; Mahlman and Moxim, 1978; Dunkerton, 1978). Mahlman (1969) indicated that the role played by eddies in modeling tracer transport can be reduced substantially by utilizing a proper averaging procedure. Three

different approaches have been developed with this particular intention: the Lagrangian mean formulation, transformed Eulerian mean approach, and the use of isentropic coordinates.

In the Lagrangian mean approach, the two-dimensional formulation is achieved by averaging the relevant parameters with respect to a material tube instead of taking a simple zonal average along a latitude circle on a constant height or pressure surface. The motion of the center of mass of such a material tube is defined to be the Lagrangian-mean motion. Based on this definition of the mean, one can see that the eddy fluxes disappear completely from the averaged transport equation. Therefore, the Lagrangian mean meridional circulation is consistent with the Brewer-Dobson circulation (Dunkerton, 1978; Matsuno, 1980). It should be noted, however, that there are practical problems in applying this formulation directly to the tracer transport (McIntyre, 1980; Schoeberl, 1981).

In the transformed Eulerian formulation, a residual mean circulation is defined as the difference between the Eulerian mean circulation and the eddy-induced mean circulation (Andrews and McIntyre, 1976). As a result, there are no eddy terms that appear explicitly in the heat and species transport equation as

long as the linear wave is steady and adiabatic and the species is conservative. In fact, when these conditions are satisfied, the rate of change of the mean potential temperature following the residual circulation is equal to the diabatic heating rate, and the residual mean circulation may be interpreted as the diabatic circulation (Holton, 1981). Furthermore, under these conditions, the transformed Eulerian mean circulation is the same as the Lagrangian-mean circulation (Dunkerton, 1978). It also has been shown that when these conditions are approximately satisfied, the calculated residual circulation appears to be a reasonable representation (Holton, 1981). However, the residual circulation does not, in general, agree with the zonally averaged mass circulation (Matsuno and Nakamura, 1979; Schoeberl, 1981).

As to the use of isentropic coordinates, Mahlman et al. (1981, 1984) and Tung (1982) have suggested that this can be the simplest conceptual approach in a two-dimensional analysis of the tracer transport in the stratosphere. In this approach, as opposed to the Lagrangian mean approach, in which the rules of eddy are completely eliminated by averaging along a material tube, isentropic coordinates are substantially reduced due to the fact that air parcels cannot cross the constant isentropic surface unless nonadiabatic processes are involved. As a result,

quasi-adiabatic wave disturbances can only introduce horizontal eddy displacements, not vertical ones, as they propagate through the stratosphere. The analysis shows that in the isentropic coordinates, the mean diabatic heating rates directly give the mean diabatic vertical velocity, with no eddy fluxes or temperature advection terms appearing in the mean energy equation (Tung, 1982). Furthermore, the mean diabatic circulation is thermally direct in the sense that the motion is upward in regions of net diabatic heating and downward in the part of the atmosphere that cools, as implicated by the Brewer-Dobson circulation based on tracer observations. These features, together with the fact that the stratosphere is largely characterized by quasi-horizontal isentropic surfaces and wave disturbances quasi-adiabatic in nature in a long-term (e.g., seasonal) time average, endow the isentropic coordinate system with a quasi-Lagrangian property (Tung, 1982). Recently, this coordinate system has been utilized in numerical simulations for nitrous oxide and nitric acid in the stratosphere by Ko et al. (1985). Perhaps one of the most practical advantages of the isentropic coordinates over the Lagrangian mean approach lies in the fact that the former can be directly applied to field measurements, while the latter is not as straightforward

(McIntyre, 1980; Tung, 1984). As a result, we have adopted the isentropic coordinate system in this study. The computational procedures and data sets will be described in detail in section 2. Section 3 presents the computed results and discussions. The summary and concluding remarks are given in section 4.

2. Computational Procedure and Data Description

A detailed two-dimensional stratospheric circulation model in an isentropic coordinate system has been formulated recently by Tung (1982) in detail. We will follow his formulation in this study to derive the diabatic circulation and to examine the associated ozone transport. A brief description of the governing equations of this diabatic circulation and the associated ozone transport is given in the first part of this section, followed by a discussion on the method of computation. A general description of the data set used in the analysis is given at the end of this section.

Governing equation:

The first law of the thermodynamics in (x, y, z) coordinate system can be written as

$$\rho_z \frac{d}{dt} \ell n \theta = \frac{q}{T}, \tag{1}$$

where ρ_z is the conventional density, mass per unit physical volume dx dy dz, and q is the diabatic heating rate, degree per unit physical volume and time. In the isentropic coordinate system, the vertical velocity, $\dot{\theta}$, is defined as

$$\dot{\theta} \equiv \frac{d}{dt} \theta, \tag{2}$$

and the density in isentropic coordinates ρ_θ, mass per unit volume dx dy dθ is related to ρ_z by the relationship,

$$\rho_\theta \equiv \rho_z \frac{\partial z}{\partial \theta}. \tag{3}$$

Define the vertical mass flow rate $W \equiv \rho_\theta \dot{\theta}$, and the static stability parameter $\Gamma \equiv \frac{T}{\theta} \frac{\partial \theta}{\partial z}$ The energy equation (i.e., Eq. 1), now becomes

$$\Gamma W = q \tag{4}$$

Equation (4) provides a direct simple relationship between the vertical mass flow rate W and the diabatic heating rate q. As opposed to the more complicated expression of energy equation in the height or pressure vertical coordinate system, which involves also horizontal temperature advection, Eq. (4) possesses a chief computational advantage over the convection Eulerian formulation (Tung, 1982).

Taking the zonal average, Eq. (4) yields

$$\bar{W}\,\bar{\Gamma} + \overline{W'\Gamma'} = \bar{q}. \tag{5}$$

The corresponding perturbation equation is found to be

$$W'\bar{\Gamma} + \bar{W}\,\Gamma' = q', \tag{6}$$

or

$$W' = \frac{q'}{\bar{\Gamma}} - \bar{W}\frac{\Gamma'}{\bar{\Gamma}}. \tag{7}$$

Equation (7) suggests that the departure of the vertical mass flow rate from the zonal mean arises as a result of variations of

the diabatic heating rate and the static stability in the longitudinal direction. It was argued that in the stratosphere, both the variations of q' and Γ's are sufficiently smaller than their zonal mean counterpart, so that the mean energy equation can be approximated (Tung, 1982) by

$$\bar{\Gamma}\,\bar{w} = \bar{q} \ , \qquad \text{or} \qquad \bar{w} = \frac{\bar{q}}{\bar{\Gamma}} \ , \tag{8}$$

To derive the meridional component of mass flow rate, we define

$$\bar{v} \equiv -a\int_{-90^\circ}^{\psi} \frac{\partial}{\partial\theta}\,(\bar{w})\,\cos\phi\ d\,\phi \ , \tag{9}$$

where ψ is the latitude, and a the earth radius. Essentially, Eq. (9) is the integrated form of the mass conservation equation in isentropic coordinates with the omission of the effect due to the transient time changes in mean density (i.e., $\frac{\partial \rho_\theta}{\partial t}$). This effect should be small in a seasonal time average (Tung, 1982). It should be mentioned that the mean diabatic circulation is completely defined by ($\bar{v}$, $\bar{w}$) given by Eqs. (9) and (8), respectively. This diabatic circulation is only slightly different from the one given by Tung [1982, Eqs. (14) and (15)], who has introduced the radiative equilibrium Γ° in place of $\bar{\Gamma}$ in

Eq. (8). The expressions of $\bar{W}$ and $\bar{V}$, given by Eqs. (8) and (9), also define a nondivergent circulation with a stream function $\bar{\psi}$ such that

$$\frac{\partial}{\partial y}\,\bar{\psi} = \bar{W},$$

$$\frac{\partial}{\partial \theta}\,\bar{\psi} = \bar{V}. \qquad (10)$$

Tung (1982) has shown that in the absence of transient eddy dispersion, the isopleths of the stream function are also the isopleths of the zonal mean mass mixing ratio ($\bar{X}$) of a conservative tracer. As indicated in the Introduction, the distribution of atmospheric tracers, especially the conservative species, are directly related to diabatic circulation. In this study, we will examine also the effect of diabatic circulation on the ozone transport and its seasonal variations.

To a good approximation, when the eddies are quasi-adiabatic and quasi-geostrophic, the general equation of mass conservation of a particular species under consideration has the simple form (Tung, 1982).

$$\bar{\rho}_\theta \frac{\partial \bar{X}}{\partial t} + \left(\bar{V}\frac{\partial \bar{X}}{\partial y} + \bar{W}\frac{\partial \bar{X}}{\partial \theta}\right) - \frac{\partial}{\partial y}\left(\bar{\rho}_\theta D_{yy}\frac{\partial}{\partial y}\bar{X}\right) = \bar{\rho}_\theta \bar{S}, \qquad (11)$$

where $y = a\sin(\phi)$; D_{yy}, a dispersion effect due to transient eddies; S is the chemical source term. Equation (11) states a balance between the local rate of change of the mean, the change

due to adiabatic circulation, the diffusion contribution, and the rate of net chemical production. As a diagnostic analysis the seasonal variations of the ozone transport associated with the diabatic circulation $(\overline{W},\overline{V})$ will be examined utilizing observational data. More specifically, the magnitude of the flux divergence of ozone concentration given by the term

$$\overline{V}\,\frac{\partial\overline{X}}{\partial y} + \overline{W}\,\frac{\partial\overline{X}}{\partial\theta}$$

will be determined in this analysis.

In determining $\overline{W}$, $\overline{V}$, and $(\overline{V}\,\frac{\partial\overline{X}}{\partial y} + \overline{W}\,\frac{\partial\overline{X}}{\partial\theta})$, the following steps have been taken:

1. Meridional distributions of the seasonal mean diabatic heating, q calculated;

2. Meridional distributions of the corresponding mean static stability determined; and

3. Meridional distributions of $\overline{W}$, $\overline{V}$, and $(\overline{V}\,\frac{\partial\overline{X}}{\partial y} + \overline{W}\,\frac{\partial\overline{X}}{\partial\theta})$ derived.

The zonal mean seasonal net heating rate, $\bar{q}$, is determined by adapting the radiative transfer model of Ramanathan (1976). The one-dimensional model extends from the ground to about 55 km in altitude. Both the long- and short-wave contributions due to O_3, H_2O, and CO_2 are included. The model accounts for the effects of surface and cloud reflections and Rayleigh scattering to the short-wave radiation, and also the Doppler-broadening effects for CO_2 and O_3 to the long-wave transfer. In addition, the exchange of infrared (IR) radiation between the level under consideration and the layers below is also included. The albedos of Rayleigh scattering and cloud are a function of solar zenith angle. In this study, the mean solar zenith angle and fractional length of daytime are determined by the third approximation of Cogley and Borucki (1976).

For the data sets, the entire SAGE 34-month ozone density profile (from February 1979 to November 1981) is used to establish the representative climatological meridional ozone distributions on a seasonal basis. These data sets are first grouped seasonally and binned into 10^{o} latitude bins. A zonal averaging procedure is then applied to each seasonal data set at

assigned constant isentropic surfaces. Similarly, the corresponding mean pressures of these surfaces are determined. This information allows us to convert relevant physical quantities from constant isentropic levels to constant pressure levels. By adapting Ramanathan's 1976 model, the solar heating and IR cooling at 11 pressure levels between 50 and 0.5 mb are determined. In the analysis, the concentrations of CO_2 and H_2O are assumed to be uniformly distributed with 320ppmv and 3ppmm, respectively. Although the effect of clouds on the net radiative heating in the stratosphere is secondary, a mean cloud-top altitude of 6 km and a mean fraction cloud cover of 0.45 are used in the analysis.

The SAGE satellite instrument utilizes the solar occultation technique to measure the attenuated solar intensity profile during spacecraft sunrise and sunset, with a vertical resolution of about 1 km. The ozone concentration profiles are deduced from measurements at the 0.6 μm channel, which is centered at the peak of the Chappius ozone absorption band. Due to the orbital characteristics of the satellite (AEM-2), the SAGE instrument provides about 30 O_3 profiles daily, corresponding to 15 spacecraft sunrises and 15 sunsets. Successive sunrise or sunset events are characterized by a 24^{o} shift in longitude and a slight

shift in latitude of about 0.2^{o} - 0.3^{o}, depending on latitude with large value of latitudinal shift in the tropics. The SAGE instrument provides a latitudinal coverage of measurements from about 70^{o}S to 70^{o}N, depending on the season. It takes about a 4-week period for the measurements to move from one latitudinal extreme to the other. Figure 1 shows the sunset event latitudinal coverage for the entire 34 months of SAGE measurements. Because of spacecraft power system deficiencies after July 1979, there are only 6 months of SAGE sunrise measurements, from February 1979 to July 1979. A detailed description of the SAGE program has been given by McCormick et al. (1979). The comparison of these SAGE-derived ozone concentrations and other types of ozone instrument measurements, including both conventional and satellite observations, has been reported with good agreement in several investigations (e.g., McCormick et al., 1984). The SAGE ozone measurements have been employed in the analysis of planetary wave transport of ozone (Wang et al., 1983), and behavior of ozone during northern warmings (Wang and McCormick, 1985), and to derive the radiative damping rate in the stratosphere (Ghazi et al., 1985).

Figure 2 shows the results of the derived seasonal climatological mean meridional distributions of ozone mass mixing

ratio (ppmm) (solid lines). The dashed lines are the corresponding constant potential temperatures derived from the meteorological information provided by NOAA's National Meteorological Center (NMC). This information is interpolated at SAGE measurement locations and times based on the NMC's routine operational analyses (Gelman et al., 1981). The solid diamonds are locations of the seasonal mean tropopause, which are also derived from data provided by NMC. Figure 2 indicates many interesting features. First of all, in the upper stratosphere above 38 km, the seasonal mean ozone mass mixing ratio is nearly horizontally stratified and the contours are approximately parallel to those of the mean potential temperature for all four seasons. It is well known that this is a region in which the climatological ozone concentration is largely under photochemical control and the effect of dynamics is secondary (Dutsch, 1971; Blake and Lindzen, 1973). Between altitudes of about 28 to 38 km, the mean ozone mixing ratio distribution exhibits a maximum centered at an altitude of about 32 km nearly above the equator. It is generally believed that the tropics region between altitudes 20 and 35 km is the main ozone source region. Stratospheric ozone is photochemically produced here and subsequently distributed through transport processes (e.g.,

Dutsch, 1971). It has been shown that the model ozone concentration in this region is strongly sensitive to circulation features, changing overhead sun-angle, and temperature (Mahlman et al., 1980). Below about 30 km, the contours of the climatological ozone concentration show generally a convex pattern. Furthermore, the distribution of the lower stratospheric ozone in the winter high latitudes is characterized by a greater poleward and downward slope than that of the constant potential temperature. (See the contours of 6 ppmm and 600°k for example in Fig. 2.) This slope relationship has been noted early in the literature (e.g., Hering, 1966; Newell, 1963). Tung (1982) is able to provide a simple and direct explanation of this feature by arguing that the air masses are being transported across the constant isentropic surface due to net radiative cooling in these regions during the winter season. At an altitude of approximately 15 km, however, ozone contours consistently show a greater slope than that of potential temperature year round at high latitudes, with change only in magnitude.

In this study, we have used the seasonal climatological mean ozone distributions depicted in Fig. 2 in conjunction with the assumed CO_2 and H_2O concentrations mentioned earlier to derive the net radiative heating $\bar{q}$. The interpolated meteorological

information at the SAGE measurement locations and times provided by NMC were used to derive the seasonal zonal mean thermal structure, $\bar{T}$, as well as the mean static stability at 11 isentropic levels from 500° to 2000° K at an increment of 150° K. The computation of $\bar{W}$ from $\bar{q}$ and $\bar{\Gamma}$ [Eq.(8)] is straightforward. However, there is some difficulty in the application of Eq. (9) to determine $\bar{V}$. Since the SAGE ozone observations do not reach to the polar region, it is necessary to extrapolate the derived meridional distribution of $\bar{W}$ to the poles. Furthermore, in order to ensure mass conservation in the analysis, a small correction Δ is added to $\bar{W}$ at each isentropic level, such that

$$\frac{\partial}{\partial \theta} \int_{-\pi/2}^{\pi/2} (\bar{W} + \Delta) \cos\phi \, d\phi = 0. \qquad (12)$$

The computed $\bar{W}$ fields were then used to calculate $\bar{V}$ and the seasonal mean stream function ψ, and $(\bar{\bar{V}} \frac{\partial \bar{\bar{X}}}{\partial y} + \bar{\bar{W}} \frac{\partial \bar{\bar{X}}}{\partial \theta})$. The results of the calculation are presented in the next section.

3. Results

For convenience, the calculated results and discussions are presented in seasonal order. In addition, the results of radiative heating and cooling are described in pressure coordinates in the conventional manner.

a. March-April-May (MAM)

The seasonal mean meridional temperature distribution for the case of MAM is given in Fig. 3a at pressure levels from 50 to 0.5 mb. It shows an approximate symmetric distribution with respect to the equator, except near the polar region in the upper stratosphere where relatively higher temperatures are found near the north pole. This feature could be attributed to the results of stratospheric warmings which occur generally during late winter and early spring in the northern hemisphere (e.g., Schoeberl, 1978). The seasonal mean meridional distribution of solar heating due to absorption of incoming solar radiation by O_3, CO_2, and H_2O corresponding to this particular season is shown in Fig. 3b. It exhibits a rather symmetric distribution, with the peak values centered at a 1 mb pressure level. A maximum heating

of about 12^{o}K/day is located above the tropics. The calculated mean distribution of IR radiation is displayed in Fig. 3c. The mean temperature distribution in Fig. 3a is employed in this IR computation. As expected, the temperature and the calculated IR cooling show quite similar contour patterns, especially in the upper stratosphere. This feature is primarily due to the strong temperature-dependent emission of the 15 μm bands of CO_2 and 9.6 μm band of O_3 (e.g., Ghazi, 1977). The derived mean net radiative heating, $\bar{q}$, is given in Fig. 3d. In general, $\bar{q}$ shows approximately a symmetric distribution with respect to the equator except in the upper stratosphere above 2 mb. It also shows a strong cooling in the region poleward of 60^{o}N with a peak (-4^{o}C/day) centered at about 3 mb. Above 2 mb, there is a region with strong net radiative heating between latitudes 30^{o}S and 60^{o}S near 1 mb. In the following presentation, the results of calculated diabatic circulation and associated ozone transport are displayed in isentropic coordinates.

The derived mean vertical mass flow rate $\bar{W}$ for the northern spring season is displayed in Fig. 4a. It shows three distinct regions with the ascending motion located at low latitudes (below $\sim 40^{o}$) and descending motion at high latitudes in both hemispheres. Note also the rapid decrease in the vertical mass

flow rate with the potential temperature. The corresponding results of the mean meridional mass flow rate $\overline{V}$ are given in Fig. 4b. They indicate that the northern hemisphere is characterized by northward flow while the southern hemisphere is dominated by southward flow. The northward flow system also shows its slight extension to the southern hemisphere in the upper stratosphere. Figure 4c shows the calculated results of seasonal mean stream function $\overline{\psi}$. It indicates distinctively a two-cell pattern, with the ascending branch located in the tropics and the descending branch at high latitudes. Thus, this circulation behavior is thermally direct. At the 500^{o}K isentropic level, these branches are separated approximately at latitudes $\pm 45^{o}$. Note also a slight hemispheric asymmetric of the cells in the upper stratosphere above about the 1400^{o}K isentropic level. This feature is also revealed in the circulation pattern implicated from LIMS H_2O measurements in May 1979 (Remsberg et al., 1984). The transport effect of this MAM diabatic circulation on the ozone concentration is given in Fig. 4d in terms of air density weighted flux divergence of the ozone mass mixing ratio. The positive/negative value of this flux divergence implies a time rate of decrease/increase of ozone concentration due to the transport effect of diabatic circulation. In the region between

about 500^{O} and 950^{O}K isentropic levels, Fig. 4d reveals positive ozone flux divergence at low latitudes and negative at high latitudes in both hemispheres. Between 950^{O} to 1250^{O}K, the stratosphere is largely characterized by weak negative values. Above 1250^{O}K, the stratosphere reveals again three different regions with weak negative flux divergence at low latitudes and positive at high latitudes. Distribution of the flux divergence in Fig. 4d can be easily understood by referring to Figs. 2a and 4c. On examining Figs. 2a, 4c, and 4d, one finds that in the lower stratosphere, the positive/negative ozone flux divergence can be attributed to the ascending/descending motion in that region where ozone concentration increases with the isentropic coordinate. In contrast, in the upper stratosphere, the ozone gradient is reversed (Fig. 2a). As shown in Fig. 4d, the signs of the flux divergence in the ascending and descending regions are changed accordingly. In Fig. 4d, the ozone transport effect of diabatic circulation is expressed in terms of air density weighted flux divergence of the ozone mass mixing ratio. Due to the exponentially decreasing nature of air density with altitude, this effect is relatively more emphasized in the lower stratosphere than in the upper stratosphere. The results of the circulation effect in terms of the ozone mass mixing ratio are

displayed in Fig. 4e. By comparison, there is no change in the sign of the positive or negative flux divergences; however, the effect of diabatic circulation is more emphasized in the upper stratosphere where the induced diabatic circulation causes a slight decrease of the mixing ratio at low latitudes and a relatively large increase in the polar regions (Fig. 4e) .

b. June-July-August (JJA)

The seasonal mean meridional temperature distribution for the JJA case (Fig. 5a) is characterized generally by a mild downward slope of the isotherms from the southern hemisphere to the north in the stratosphere, except in the high latitude southern hemisphere (poleward of 40^{o}S). Near 40^{o}S, there is a rapid drop of temperature in the poleward direction. Between latitudes 50^{o}S and 60^{o}S, Fig. 5a also shows a poleward increase of the temperature in the upper stratosphere. Note also the maximum temperature centered at 1 mb pressure level in the northern polar region. In general, this seasonal mean temperature distribution corresponds closely to the mean temperature distribution in northern summer months reported by Barnett and Corney (1985). Figure 5b shows the results of the

computed mean solar heating for the same period. It exhibits a peak of the heating rate located at about 1 mb pressure level, with a maximum centered in the northern polar region. This heating rate distribution is found to be compatible with the results of London (1979). The corresponding results of IR cooling are given in Fig. 5c, indicates a similar contour pattern as the mean temperature distribution in the stratosphere (Fig. 5a). Note, a cooling rate maximum greater than 8^{o}K/day is located near 1.5 mb at 70^{o}N. The distribution of the mean net heating rate, $\overline{q}$, is displayed in Fig. 5d. Generally, Fig. 5d indicates excessive net heating rates in the summer hemisphere and net cooling in the winter hemisphere. In the upper stratosphere, Fig. 5d shows the extension of the positive net heating rate from the summer hemisphere into the low latitudes of the winter hemisphere. Note also the net cooling region at northern high latitudes in the lower stratosphere, a feature found in the analysis of Murgatroyd and Singleton (1961). This net cooling is most probably a consequence of strong IR cooling due to high temperature distributions. We have compared Fig. 5a with the temperature fields in the summer months reported by Barnett and Corney (1985). They show close agreement.

The calculated mean diabatic circulation for JJA is given in Figs. 6a to e. The mean vertical mass flow rate $\overline{W}$ exhibits

generally a descending motion in the winter hemisphere and an ascending motion in the summer hemisphere, except at northern high latitudes between 500° and 800°K isentropic levels (Fig. 6a). Near the lower stratospheric summer pole, the descending motion is the result of a regional net cooling (Fig. 5d) and can be attributed to the imbalance of the IR cooling near the high temperature summer pole mentioned earlier. Figure 6b is the result of mean meridional mass flow rate. Noteworthy features are the northward motion between latitudes about 20°S to 90°N, and the southward motion between 90°S and 20°S in the lower stratosphere (below 800°K). The region of this southward motion branches up toward the north pole in the layer between approximately 950° and 1250°K isentropic levels. Above 1550°K, the mean meridional mass flow shows mainly a layer of relatively weak southward flow with a local maximum center located near the 1850°K isentropic level near 15°S latitude. Furthermore, a weak layer of northward flow centered at 1400°K level extends almost from pole to pole. Figure 6c shows the corresponding results of the calculated mean stream function. It indicates a two-cell pattern below approximately the 800°K isentropic level (~30 km, Fig. 2b), with the upward branch centered near 20°N latitude at 500°K

level. In regions above 800°K, Fig. 6c reveals mainly a single-cell pattern with the center of this cell shifting slightly toward the winter hemisphere.

The seasonal mean flux divergence of the air mass weighted ozone is given in Fig. 6d. In the region below approximately the 950°K isentropic level, this figure resembles the pattern shown in Fig. 4d for the MAM case, with a positive flux divergence at low latitudes and negative values at high latitudes. In comparison, above the 1100°K level, Fig. 6d shows a region of negative flux divergence in the northern hemisphere and positive values in the south. Similarly, the mean flux divergence of ozone mass mixing ratio shows negative values in the northern upper stratosphere and positive numbers in the south (Fig. 6e). Again, the sign of ozone flux divergence is controlled by the direction of the flow of the diabatic circulation and by the ozone mass mixing ratio distribution.

c. September-October-November (SON)

The calculated mean temperature (Fig. 7a) for this period reveals a symmetric distribution with respect to the equator,

except at high latitudes beyond $\pm 50^{o}$. In fact, there is a distinct temperature minimum at 50^{o}S, as noted by Ghazi and Barnett (1980) analyzing satellite (SCR) data. At high latitudes, the mean temperature increases poleward in the upper stratosphere (~1 mb) especially near the south pole. The computed mean solar heating rate is displayed in Fig. 7b. It exhibits a distinct hemispherical symmetric pattern which resembles the MAM case (Fig. 3b). A maximum heating ~12^{o}K/day is located near 1 mb above the equator. As regards the IR cooling of this particular season, the calculated distribution is a mirror image of MAM's, although a slight difference is noticeable in the upper stratosphere. In general, the net heating rate (Fig. 7d) features a similar meridional distribution as the MAM case, except in the upper stratosphere near 1 mb. In this SON case, the maximum is centered above the equator, while in the MAM case it is centered at 50^{o}S.

Figs. 8a to e show the corresponding diabatic circulation for the SON case. In comparison, the computed vertical mass flow rate W (Fig. 8a) exhibits a symmetric pattern similar to the MAM case (Fig. 4a), with an ascending motion at low latitudes and a descending motion at high latitudes. The meridional flow rate $\overline{V}$ (Fig. 8b) reveals generally a poleward motion in both

hemispheres, except in the tropical lower stratosphere in the southern hemisphere where the meridional flow field appears to be an extension of the flow system from the northern hemisphere. The analyzed stream function $\overline{\psi}$ is displayed in Fig. 8c. Again, like the corresponding MAM case (Fig. 4c), it shows a two-cell pattern, with an upward branch in the tropics and a downward branch at the high latitudes. The calculated ozone flux divergence associated with this diabatic circulation is given in Fig. 8d. Qualitatively, the distribution of this mass weighted ozone flux divergence is similar to Fig. 4d for the MAM period; likewise the ozone mass mixing ratio flux divergence for these two seasons (Figs. 8e and 4e).

d. December-January-February (DJF)

The meridional distribution of mean temperature for the DJF case is presented in Figure 9a. It reveals generally a downslope of the temperature isoplathe from the north pole to the south pole, except at the lower stratosphere below 30 mb. In the region below 30 mb, Fig. 9a indicates a low temperature region centered at the equator. Figure 9b depicts the calculated mean solar heating rates, a hemispherical distribution reversed from

that of the JJA period (Fig. 5b). A maximum heating rate of ~14^{O} K/day is located at 1 mb near the summer pole (Fig. 9b). The corresponding IR cooling rate is given in Fig. 9c. Again, the distribution pattern of this cooling rate resembles that of the associated temperature distribution. The computed net heating rate (Fig. 9d) shows a net cooling near the winter pole. A cooling rate of -4^{O}K/day is located near 2 mb at 60^{O}N latitude. A maximum heating rate of ~6^{O}K/day is found near 1 mb above 70^{O}S latitude. At 1 mb pressure level, the positive heating rate field extends from the south pole to the northern hemisphere and reaches about 40^{O}N. In the lower stratosphere, the positive net heating is found in the region between latitudes approximately 40^{O}S and 20^{O}N and net cooling at high latitudes in both hemispheres. This situation is similar to the one for JJA (Fig. 5d) with a reversed hemispheric distribution. It should be mentioned that the results of London (1979) show a net heating distribution in the summer south polar region extending from an altitude of 20 km to 100 km. This variation is probably due to the difference in temperature distributions in that region between Fig. 9a and his. London's temperature distribution in the summer south polar region is slightly lower than the corresponding distribution in Fig. 9a and also that of Barnett and Corney (1985).

The derived results of diabatic circulation are displayed in Figs. 10a to e. The calculated vertical mass flow rate $\overline{W}$ (Fig. 10a) shows descending motions in regions northward of 10^{O}N in the stratosphere. In the stratosphere southward of 10^{O}N, the flow motion is generally upward, except at high latitudes in the lower stratosphere. The calculated mean meridional mass flow rate is given in Fig. 10b. In the lower stratosphere, it shows mainly a poleward flow in the northern hemisphere. This poleward flow system appears to extend into the southern hemisphere down to about 30^{O}S at the 500^{O}K isentropic level. In the southern hemisphere, the lower stratosphere is dominated by a southward flow system centered at 55^{O}S latitude near the 650^{O}K isentropic surface. In the upper stratosphere, north of latitude 40^{O}N, the flow is mostly northward, except in the layer centered at the 1400^{O}K isentropic level. At latitudes south of 40^{O}S, the upper stratosphere is generally characterized by southward flow. The mean stream function for the DJF period is displayed in Fig. 10c. Fig. 10c reveals mainly a two-cell pattern below the 950^{O}K isentropic level (~30 km), and a single cell pattern above. This single cell flow pattern is a hemispheric reversal of the JJA case (Fig. 6e), with a slight shift of the cell center toward the

winter hemisphere. The ozone transport effect of the diabatic circulation of the DJF case is given in Fig. 10d. In the lower stratosphere, Fig 10d shows positive values of ozone mass flux divergence at low latitudes and negative values in the high latitudes. In the upper stratosphere, Fig. 10d indicates negative values of the divergence in the winter hemisphere and positive values in the summer hemisphere. The ozone transport effect in terms of mass mixing ratio is given in Fig. 10e. Noteworthy features are the positive divergence in the northern upper stratosphere and its negative values in the south. This distribution is just the opposite of the case for the JJA period (Fig. 6e).

4. Summary and Concluding Remarks

In this study, we have investigated the seasonal variations of stratospheric diabatic circulation and the associated transport effect on ozone distributions on a diagnostic basis. The analysis is performed by using the isentropic coordinate approach formulated by Tung (1982). Ramanathan's model (1976) has been adapted for the radiative heating and cooling calculation. In the calculation, the seasonal climatology of stratospheric ozone distributions is derived from observation of the entire 34-month measurement period (from February 1979 to November 1981) of the Stratospheric Aerosol and and Gas Experiment (SAGE). The corresponding seasonal thermal structures are determined based on meteorological information (e.g., temperature) provided by NOAA for each SAGE measurement. The results indicate that in the lower stratosphere, the derived diabatic circulation exhibits basically a two-cell mass flow pattern during both equinox and solstice, and in the upper stratosphere, a single-cell pattern during solstice and a two-cell structure during equinox. The results also show a slight latitudinal shift of the center of this single cell toward the winter hemisphere. The calculated flux divergence of the air mass weighted ozone concentration associated with the derived diabatic circulation also shows

differences in the seasonal variations between the lower and the upper stratospheres. In the lower stratosphere, the calculated results show consistently positive divergence at low latitudes and negative at high latitudes for all four seasons. In the upper stratosphere during the equinox, this situation is reversed, with positive divergence at high latitudes and negative at low latitudes. During the solstice, the flux divergence is generally positive in the winter hemisphere and negative in the summer hemisphere. Due to the exponential decrease of the air density with height, the magnitudes of the flux divergence in the upper stratosphere are much smaller than those in the lower stratosphere. We have also derived the flux divergence in terms of ozone mass mixing since it is often used in the existing stratospheric ozone photochemical models. The results are similar to those expressed in the mass weighted flux divergence, although here the emphasis is more on the upper stratosphere.

It should be noted that the structure of the stratosphere is generally governed by strongly coupled processes involving dynamics, photochemistry, and radiation (e.g. Hartmann, 1981; Brasseur and Solomon, 1984). Similarly, the stratospheric ozone concentration is essentially determined by these coupled processes. Nevertheless, the seasonal climatological ozone

concentration at middle and high latitudes has been recognized to be mainly under photochemical control in the upper stratosphere and is largely dynamically controlled in the lower stratosphere (Dutsch, 1971; Blake and Lindzen, 1973; Solomon et al., 1985). By using a three-dimensional model, Cunnold et al. (1980) have shown the latitudinal variations of the vertical extent of these various ozone controlling mechanisms. As a result, although the ozone transport effect of the diabatic circulation is investigated for the entire stratosphere, this transport effect should be regarded as secondary in the upper stratosphere when compared with the contribution due to ozone photochemistry in the same region. In the lower stratosphere the ozone transport effect of the diabatic circulation has been recognized to play a significant role in determining ozone distribution on a seasonal basis. The essentially two-cell pattern of the calculated diabatic circulation in the lower stratosphere explains largely the observed persistent convex structure of ozone distributions in this region. Finally, we have examined the ozone transport effect of diabatic circulation variations. This circulation can also be incorporated into model transport analysis of other trace species in the stratosphere which are important for climate studies.

ACKNOWLEDGMENT

The authors wish to thank Drs. L. B. Callis, R. E. Boughner and E. E. Remsberg of NASA Langley Research Center and Dr. W. C. Wang of the Atmospheric and Environmental Research, Inc. for helpful comments and discussions. P.-H. Wang was supported by NASA Contracts NAS1-17032 and NAS1-17959.

REFERENCES

Andrews, D. G., and M. E. McIntyre, 1976: Planetary waves in horizontal and vertical shear: The generalized Eliassen-Palm relation and the mean zonal acceleration. J. Atmos. Sci. 33, 2031-2048.

Barnett, J. J., and M. Corney, 1985: Middle atmosphere reference model derived from satellite data, Middle Atmosphere Program Handbook, Vol. 16. Avail.: SCOSTEP Secretariat, University of Illinois, 1406 Green Street, Urbana, Illinois, 61801), edited by K. Labitzke, J. J. Barnett, and B. Edwards, 47.

Blake, D., and R. S. Lindzen, 1973: The effect of photochemical models on calculated equilibria and cooling rates in the stratosphere. Mon. Wea. Rev., 101, 783-802.

Brasseur, G., and S. Solomon, 1984: Aeronomy of the Middle Atmosphere. D. Reidel Publishing Co., 441.

Brewer, A. W. , 1949: Evidence for a world circulation provided by measurements of helium and water vapor distribution in the stratosphere. Quart. J. Roy. Meteor. Soc., 75, 351-363.

Chapman, S., and R. S. Lindzen, 1970: Atmospheric Tides, D. Reidel Press, Dordrecht, Holland, 200 pp.

Charney, J. G., and P. G. Drazin, 1961: Propagation of planetary scale disturbances from the lower into the upper atmosphere. J. Geophys. Res., 66, 83-109.

Cogley, A. C., and W. J. Borucki, 1976: Exponential approximation for daily average solar heating or photolysis. J. Atmos. Sci., 33, 1347-1356.

Cunnold, D. M., F. N. Alyea and R. G. Prinn, 1980: Preliminary calculations concerning the maintenance of the zonal mean ozone distribution in the northern hemisphere. Pure Appl. Geophys., 118, 284-306.

Dickinson, R. E., 1980: Planetary waves: Theory and observation in Orographic Effects in Planetary Flows, WMO GARP Publ. No. 23, 51-84.

Dobson, G. M. B., 1956: Origin and distribution of polyatomic molecules in the atmosphere. Proc. Roy. Soc. London, A235, 187-192.

Dunkerton, T., 1978: On the mean meridional mass motions of the stratosphere and mesosphere. J. Atmos. Sci., 35, 2325-2333.

Dutsch, H. U., 1971: Photochemistry of atmospheric ozone, Advances in Geophysics, 15, Academic Press, 219-232. 1971.

Gelman, M. E., A. J. Miller, J. D. Laver and F. G. Finger, 1981: An evaluation of stratospheric meteorological analyses using satellite sounder and rocketsonde data. Middle Atmosphere Program Handbook, Vol. 2, 1-9. (Available from SCOSTEP Secretariat, University of Illinois, 1406 W. Green St., Urbana, IL 81801).

Ghazi, A., 1977: Infrared cooling during a stratospheric warming. J. Atmos. Terr. Phys., 38, 890-895.

_____, and J. J. Barnett, 1980: Ozone behavior and stratospheric thermal structure during southern hemisphere Spring. Cont. Atm. Phys, 53, 1-13.

_____, Pi-Huan Wang, and M. P. McCormick, 1985: A study on radiative damping of planetary waves utilizing stratospheric observations. J. Atmos. Sci., 42, 2032-2042.

Hartmann, D. L., 1981: Some aspects of the coupling between radiation, chemistry, and dynamics in the stratosphere. J. Geophys. Res., 86, 9631-9640.

Hering, W. S., 1966: Ozone and atmospheric transport processes, Tellus, 18, 329-336.

Holton, J. R., 1975: The dynamic meteorology of the stratosphere and mesosphere, Meteor. Monogr., 37, Amer. Meteor. Soc., 216.

_____, 1976: A semi-spectral numerical model for wave-mean flow interactions in the stratosphere: Applications to sudden stratospheric warmings, J. Atmos. Sci., 33, 1639-1649.

_____, 1981: An advective model for two-dimensional transport of stratospheric trace species, J. Geophys. Res., 86, 11989-11994.

_____, and W. M. Wehrbein, 1980: A numerical model of the zonal mean circulation of the middle atmosphere. Pure Appl. Geophys., 118, 284-306.

Hunt, B. G., and S. Manabe, 1968: Experiments with a stratospheric general circulation model II: Large-scale diffusion of tracers in the stratosphere. Mon. Wea. Rev., 96, 503-539.

Ko, M. K. W., K. K. Tung, D. K. Weisenstein, and N. D. Sze, 1985: A zonal mean model of stratospheric tracer transport in isentropic coordinates: Numerical simulations for nitrous oxide and nitric acid, J. Geophys. Res., 90, 2313.

Leovy, C. B., 1964: Simple models of driven mesospheric circulations, J. Atmos. Sci., 21, 327-341.

London, J., 1979: Radiative energy sources and sinks in the stratosphere and mesosphere, in proceedings of the NATO Advanced Study Institute on Atmospheric Ozone: Its Variation and Human Influences. Ed. A. C. Aikin, 703-722, (NTIS).

Mahlman, J. D., 1969: Heat balance and mean meridional circulation in the polar stratosphere during the sudden warming of January 1958. Mon. Wea. Rev., 97, 534-540.

_____, and W. J. Moxim, 1978: Tracer simulation using a global general circulation model: Results from a midlatitude instantaneous source experiment, J. Atmos. Sci., 35, 1340-1374.

_____, Levy II, and W. J. Moxim, 1980: Three-dimensional tracer structure and behavior as simulated in two ozone precursor experiments, J. Atmos. Sci., 37, 655-685.

_____, D. G. Andrews, H. U. Dutsch, D. L. Hartman, T. Matsuno, and R. J. Murgatroyd, 1981: Transport of trace constituents in the stratosphere, Middle Atmosphere Program Handbook, 3. Avail.: SCOSTEP Secretariat, University of Illinois, 1406 Green Street, Urbana, Illinois, 61801, edited by C. F. Sechist, 14.

_____, _____, _____, _____, _____, _____, 1984: Transport of trace constituents in the stratosphere, Dynamics of the Middle Atmosphere, Advances in Earth and Planetary Sciences, edited by J. R. Holton and T. Matsuno, 387, Terra Scientific Publishing Co., Tokyo.

Matsuno, T., 1971: A dynamical model of the stratospheric sudden warming. J. Atmos. Sci., 28, 1479-1494.

_____, 1980: Lagrangian motion of air parcels in the stratosphere in the presence of planetary waves. Pure Appl. Geophys., 118, 189-216.

_____, and K. Nakamura, 1979: The Eulerian- and Lagrangian-mean meridional circulations in the stratosphere at the time of a sudden warming. J. Atmos. Sci., 36, 640-654.

McCormick, M. P., T. J. Pepin, W. P. Chu, T. J. Swissler and L. R. McMaster, 1979: Satellite studies of the stratospheric aerosol, Bull. Amer. Meteor. Soc., 60, 1038-1046.

_____, T. J. Swissler, E. Hilsenrath, A. J. Krueger and M. T. Osborn, 1984: Satellite and correlative measurements of stratospheric ozone: Comparison of measurements made by SAGE, ECC balloons, chemiluminescent, and optical rocketsondes. J. Geophys. Res., 89, 5315-5320.

McIntyre, M. E., 1980: Towards a Lagrangian-mean description of stratospheric circulations and chemical transports. Phil. Trans. Roy. Soc. London., A296, 129-148.

Murgatroyd, R. T., and F. Singleton, 1961: Possible meridional circulations in the stratosphere and mesosphere. Quart. J. Roy. Meteor. Soc., 87, 125-135.

Newell, R. E., 1963: The circulation of the upper atmosphere. Sci. Amer., 210, 62-74.

Quiroz, R. S., 1979: Tropospheric-stratospheric interaction in the major warming event of January-February 1979. Geophys. Res. Lett., 6, 645-648.

Ramanathan, V., 1976: Radiative transfer within the earth's troposphere and stratosphere: A simplified radiative-convective model. J. Atmos. Sci., 33, 1330-1346.

Remsberg, E. E., J. M. Russell III, L. L. Gordley, J. C. Gille, and P. L. Bailey, 1984: Implications of the Stratospheric Water Vapor distribution as determined from the Nimbus 7 LIMS experiment. J. Atmos. Sci., 41, 2934-2945.

Schoeberl, M. R., 1978: Stratospheric warmings: Observations and theory. Rev. Geophys. Space Phys., 16, 521-538.

_____, 1981: A simple model of the Lagrangian-mean flow produced by dissipating planetary waves. J. Atmos. Sci., 38, 1841-1855.

_____, and D. F. Strobel, 1980: Numerical simulation of sudden stratospheric warmings, J. Atmos. Sci., 37, 214-236.

Solomon, S., R. R. Garcia, and F. Storrdal, 1985: Transport Processes and ozone perturbations. J. Geophys. Res., 90, 12981-12989.

Tung, K. K., 1982: On the two-dimensional transport of stratospheric trace gases in isentropic coordinates, J. Atmos. Sci., 39, 2330.

_____, 1984: Modeling of tracer transport in the middle atmosphere, Dynamics of the Middle Atmosphere, Advances in Earth and Planetary Sciences, edited by J. R. Holton and T. Matsuno, 417, Terra Scientific Publishing Co., Tokyo.

Wang, P., and P. McCormick, 1985: Variations in stratospheric aerosol optical depth during northern warmings, J. Geophys. Res., 90, 10597-10606.

_____, _____, and W. P. Chu, 1983: A study on the planetary wave transport of ozone during the late February 1979 stratospheric warming using the SAGE ozone observation and meteorological information. J. Atmos. Sci., 40, 2419-2431.

FIGURE CAPTIONS

Figure 1 Latitudinal coverage of SAGE sunset measurements (February 1979-November 1981).

Figure 2 Seasonal distribution of zonal mean stratospheric ozone mass mixing ratio in unit ppmm (solid lines), constant potential temperature (dashed lines). Solid diamonds are the locations of aerosol mean tropopause.

Figure 3 Northern-spring distribution of zonal mean (a) temperature (^{o}K); (b) solar heating (^{o}K/day); (c) IR cooling (^{o}K/day); and (d) net heating (^{o}K/day).

Figure 4 Northern-spring distributions of (a) vertical velocity in unit (cm/^{o}K)(gm/cm^{3})(^{o}K/sec) scaled by 10^{6} with a contour interval of 20; (b) meridional velocity in unit (cm/^{o}K)(gm/cm^{3})(m/sec) scaled by 10^{2}, (c) stream function in unit (cm/^{o}K)(gm/cm^{3}) (1/sec) scaled by 10^{-2} (d) mass weighted O_3 flux divergence due to diabatic circulation in unit (cm/oK)(gm/cm3) (1/sec) scaled by 108 and (e) O_3 (mass mixing ratio) flux divergence in unit (1/sec) scaled by 10^{-6}.

Figure 5 The same as Figure 3 except for season JJA.

Figure 6 The same as Figure 4 except for season JJA.

Figure 7 The same as Figure 3 except for season SON.

Figure 8 The same as Figure 4 except for season SON.

Figure 9 The same as Figure 3 except for season DJF.

Figure 10 The same as Figure 4 except for season DJF.

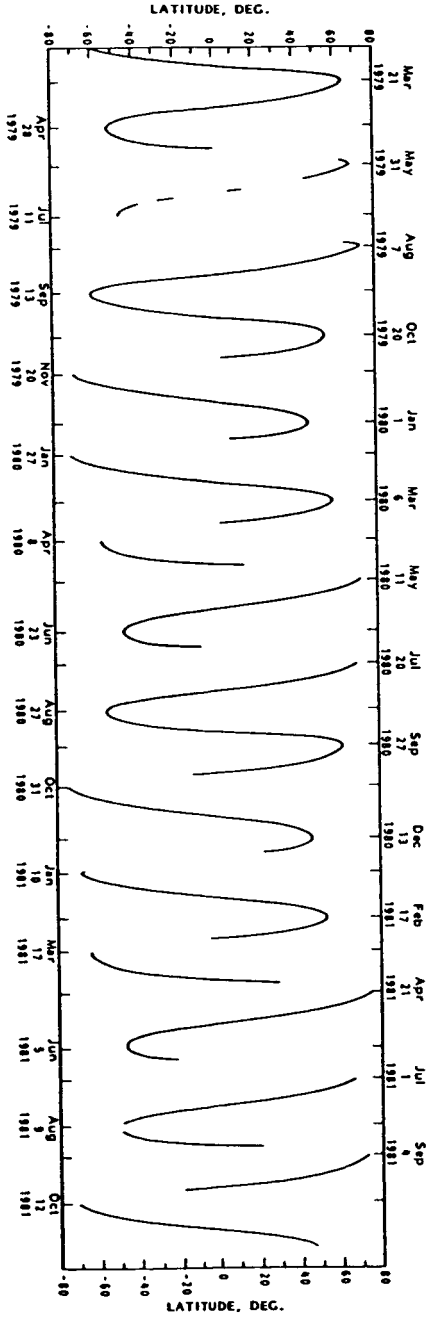

Figure 1

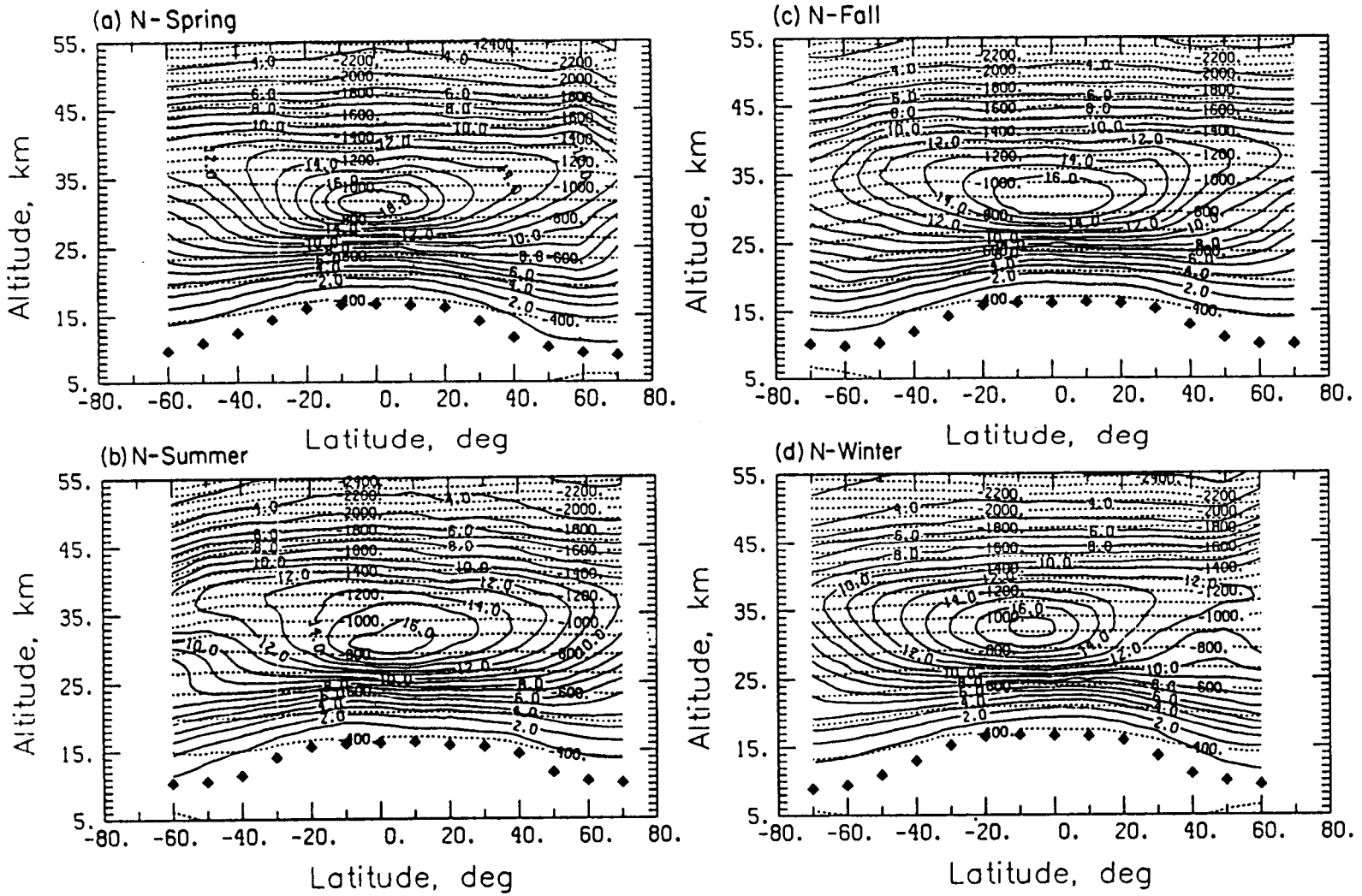
(a) N-Spring
(b) N-Summer
(c) N-Fall
(d) N-Winter
Altitude, km
Latitude, deg
55.
45.
35.
25.
15.
5.
-80. -60. -40. -20. 0. 20. 40. 60. 80.

Figure 2

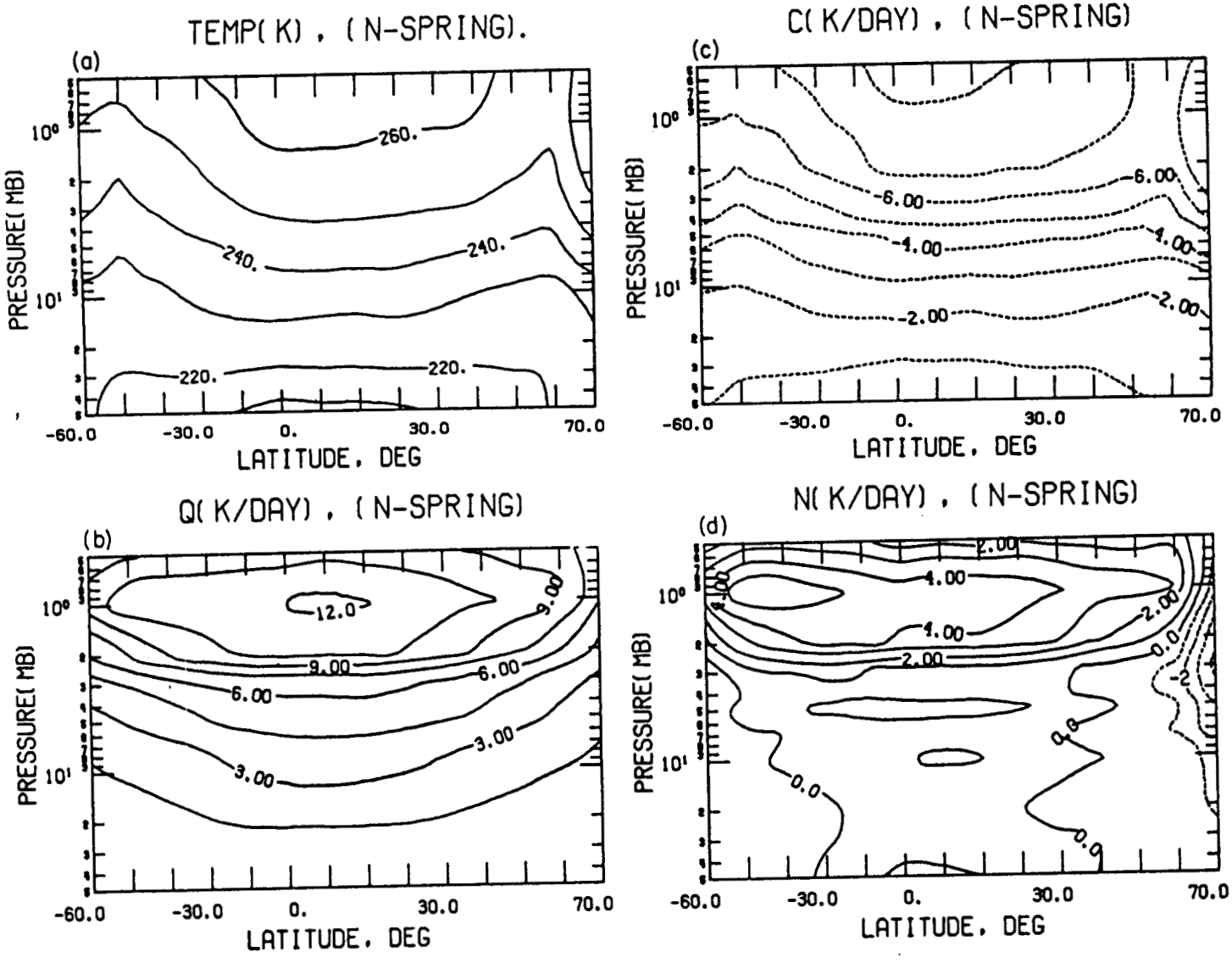
TEMP(K) , (N-SPRING).
(a)
260.
240.
240.
220.
220.
PRESSURE(MB)
LATITUDE, DEG
C(K/DAY) , (N-SPRING)
(c)
6.00
6.00
4.00
4.00
2.00
2.00
PRESSURE(MB)
LATITUDE, DEG
Q(K/DAY) , (N-SPRING)
(b)
12.0
9.00
9.00
6.00
6.00
3.00
3.00
PRESSURE(MB)
LATITUDE, DEG
N(K/DAY) , (N-SPRING)
(d)
4.00
2.00
4.00
2.00
0.0
0.0
0.0
PRESSURE(MB)
LATITUDE, DEG

Figure 3

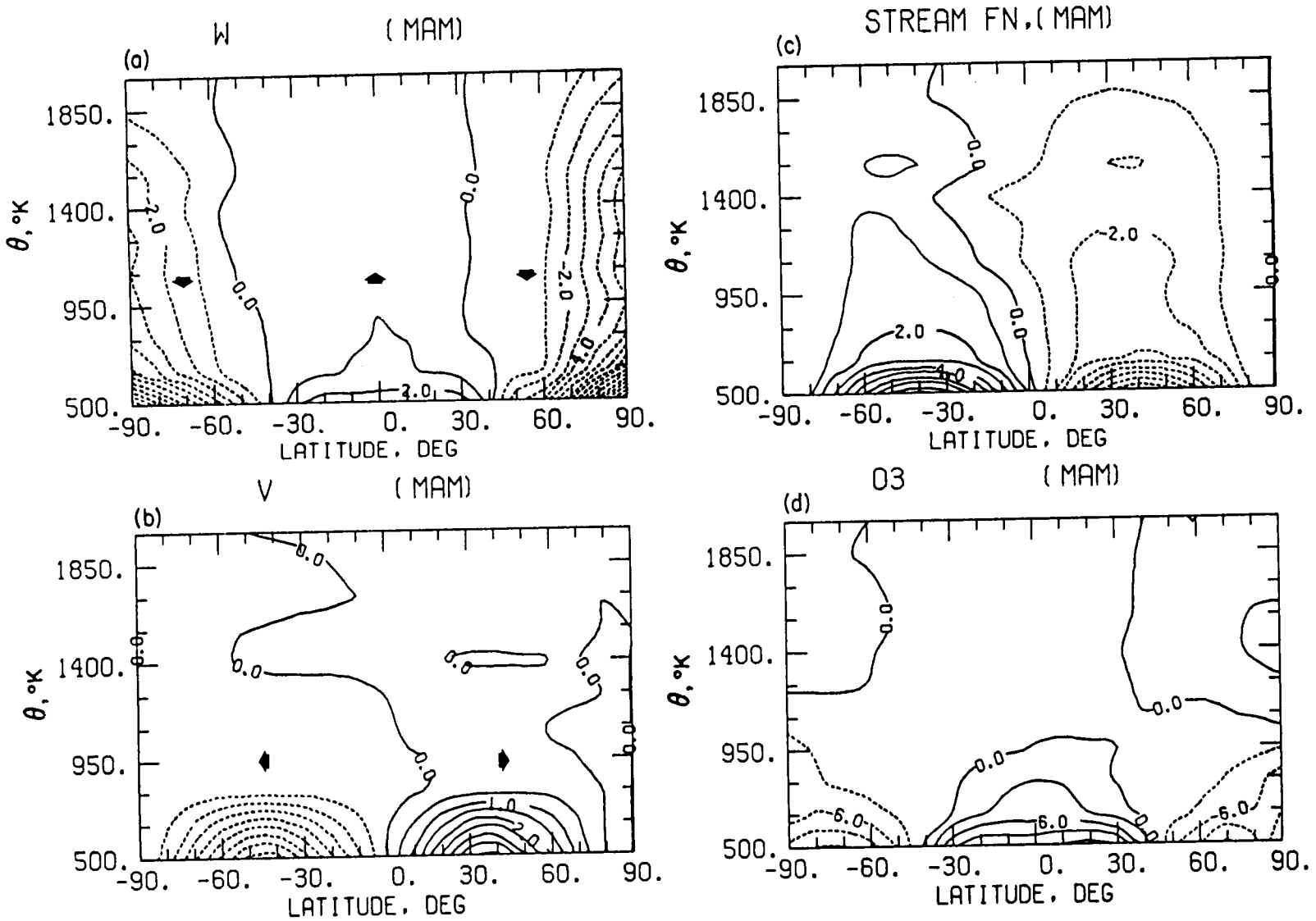
W (MAM)
(a)
1850.
1400.
950.
500.
θ, °K
-90. -60. -30. 0. 30. 60. 90.
LATITUDE, DEG
STREAM FN.(MAM)
(c)
V (MAM)
(b)
O3 (MAM)
(d)

Figure 4

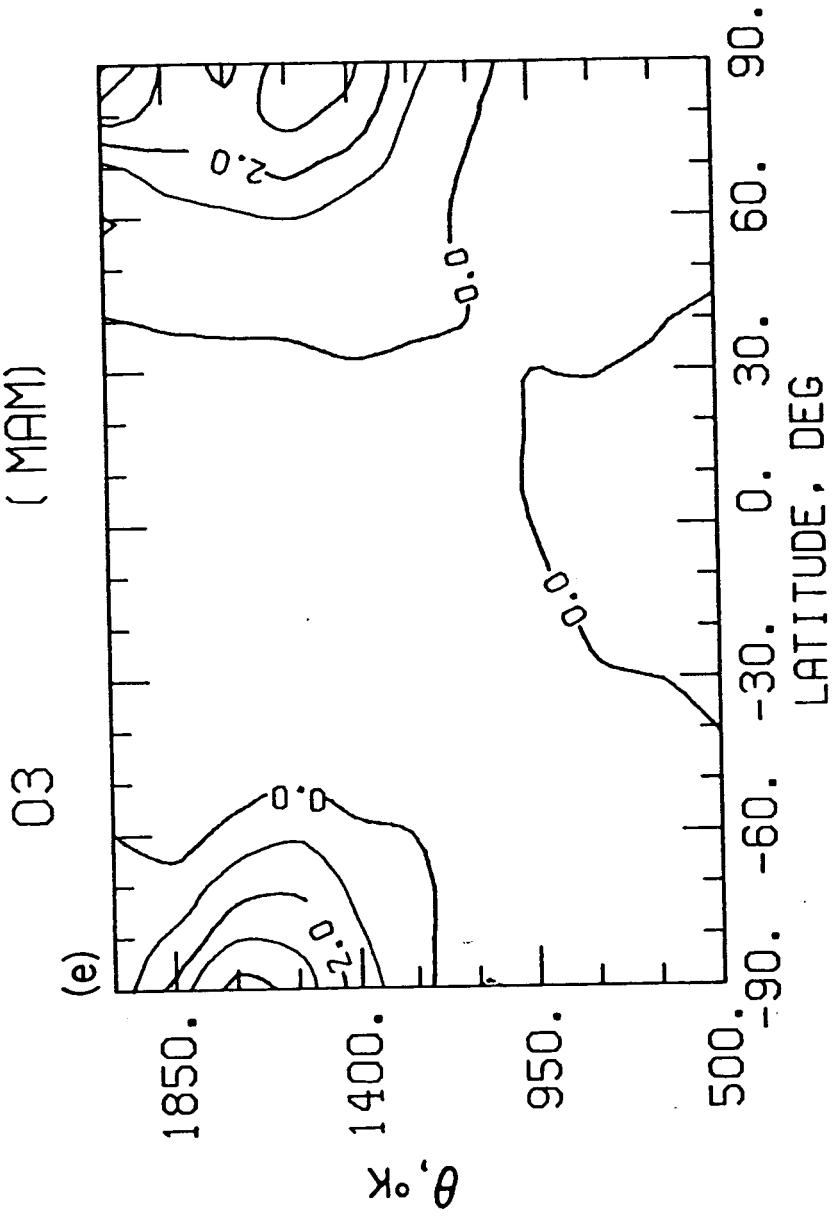
(e)
O3
(MAM)
θ, °K
1850.
1400.
950.
500.
-90.
-60.
-30.
0.
30.
60.
90.
LATITUDE, DEG
0.0
2.0
0.0
0.0
0.2
0.0

Figure 4e

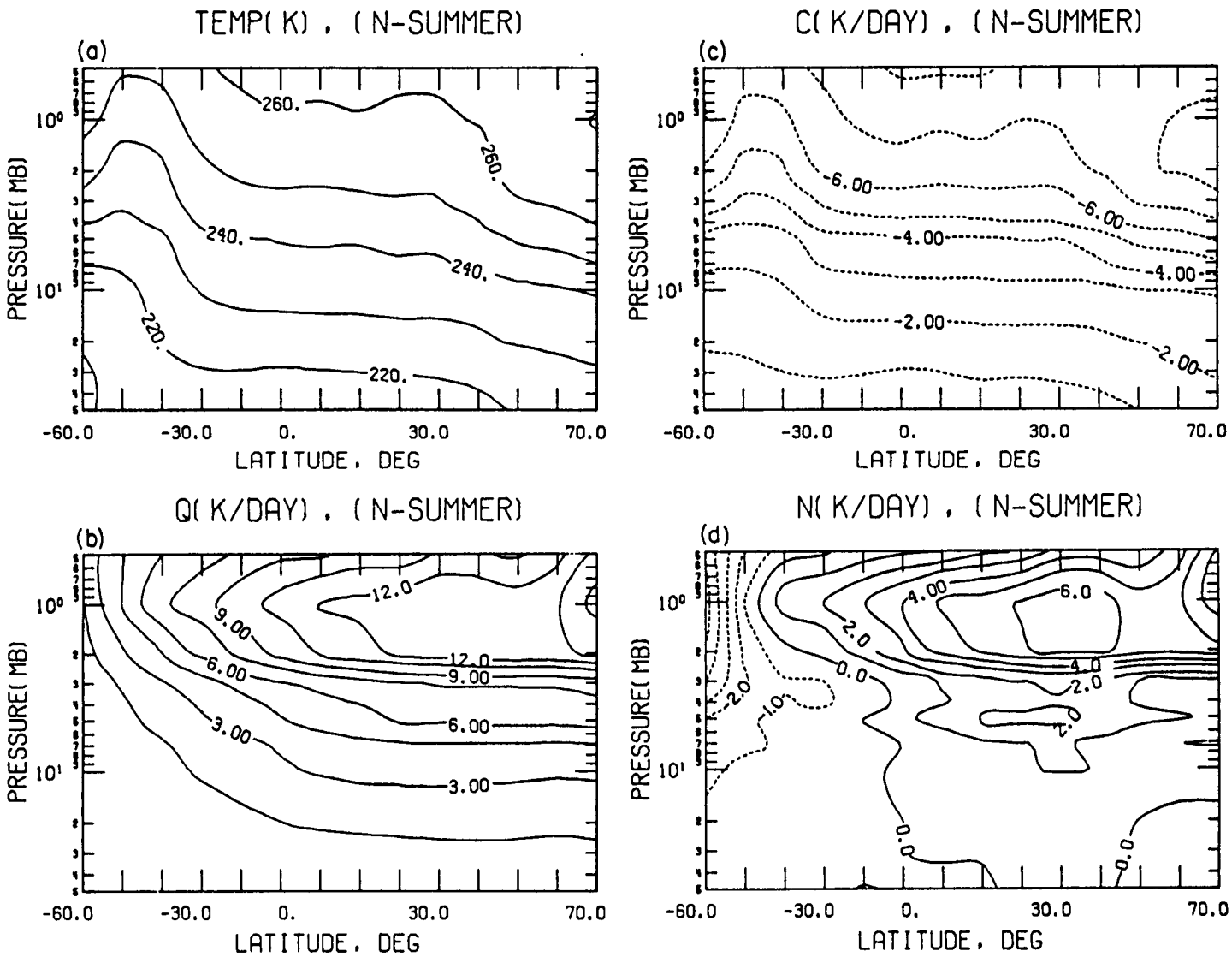
TEMP(K) , (N-SUMMER)
(a)
260.
240.
220.
PRESSURE(MB)
LATITUDE, DEG
C(K/DAY) , (N-SUMMER)
(c)
-6.00
-4.00
-2.00
Q(K/DAY) , (N-SUMMER)
(b)
12.0
9.00
6.00
3.00
N(K/DAY) , (N-SUMMER)
(d)
6.0
4.00
2.0
0.0
-2.0
-60.0
-30.0
0.
30.0
70.0

Figure 5

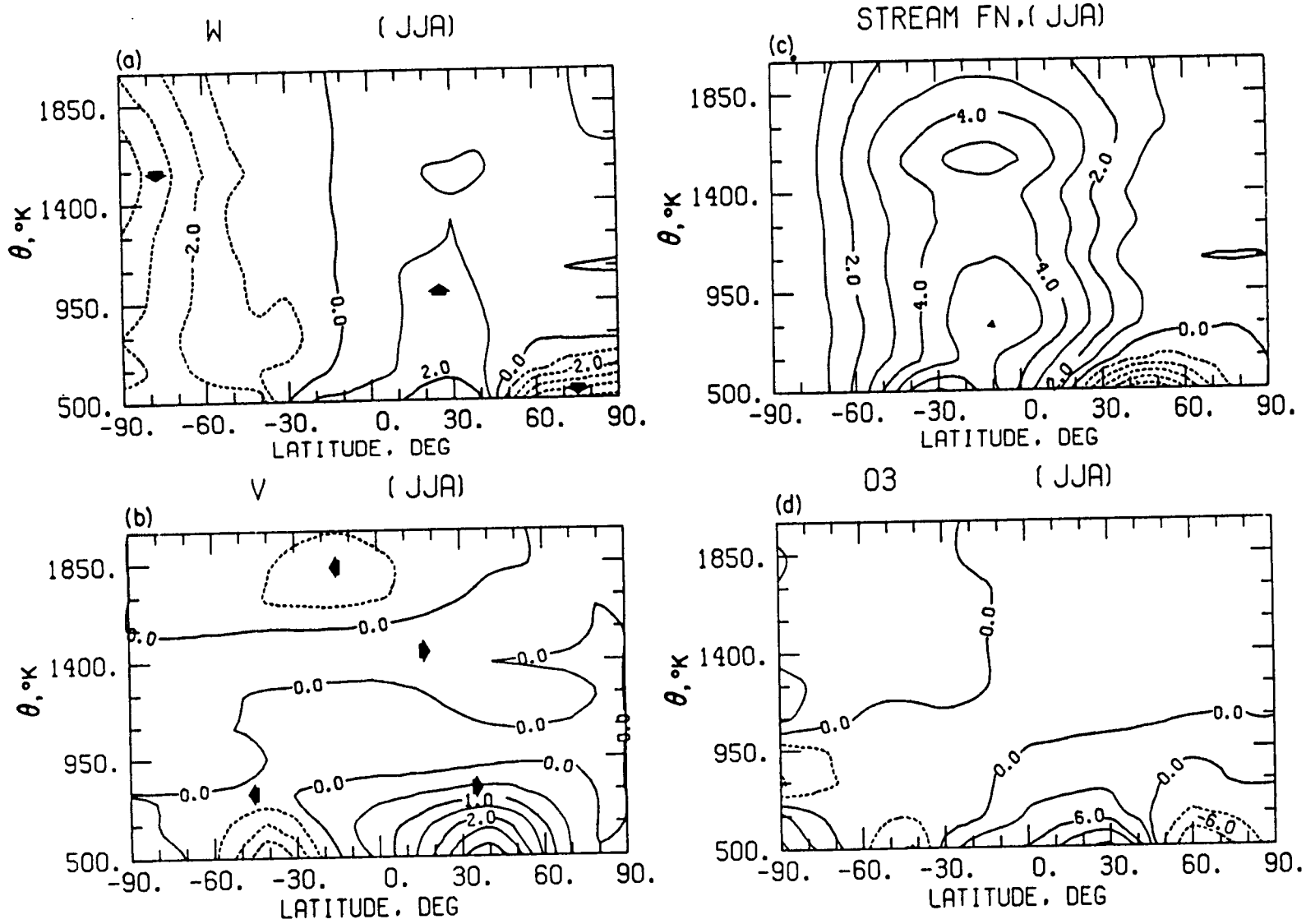
W (JJA)
(a)
1850.
1400.
950.
500.
θ, °K
-90. -60. -30. 0. 30. 60. 90.
LATITUDE, DEG
STREAM FN.(JJA)
(c)
4.0
2.0
0.0
V (JJA)
(b)
1.0
-2.0
O3 (JJA)
(d)
6.0
-6.0

Figure 6

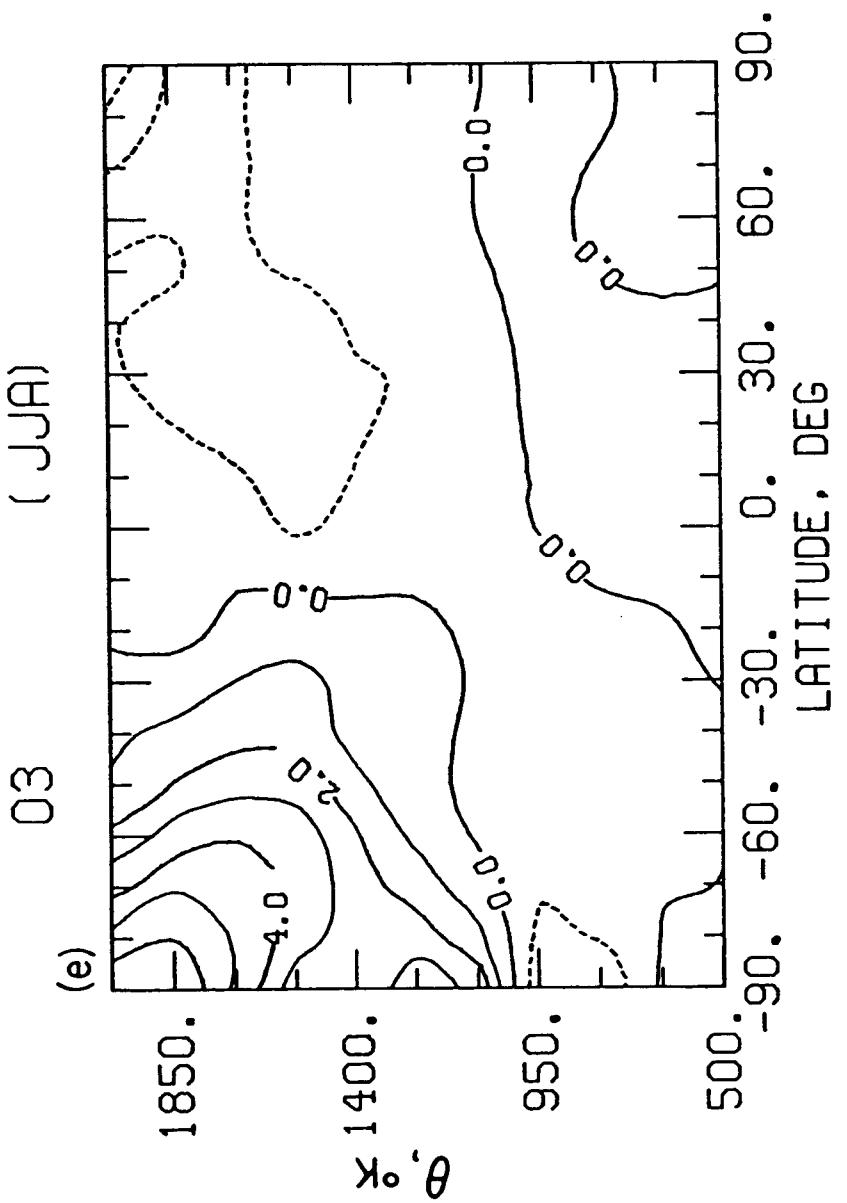
(e)
03
(JJA)
4.0
2.0
0.0
0.0
0.0
0.0
1850.
1400.
950.
500.
θ, °K
-90.
-60.
-30.
0.
30.
60.
90.
LATITUDE, DEG

Figure 6e

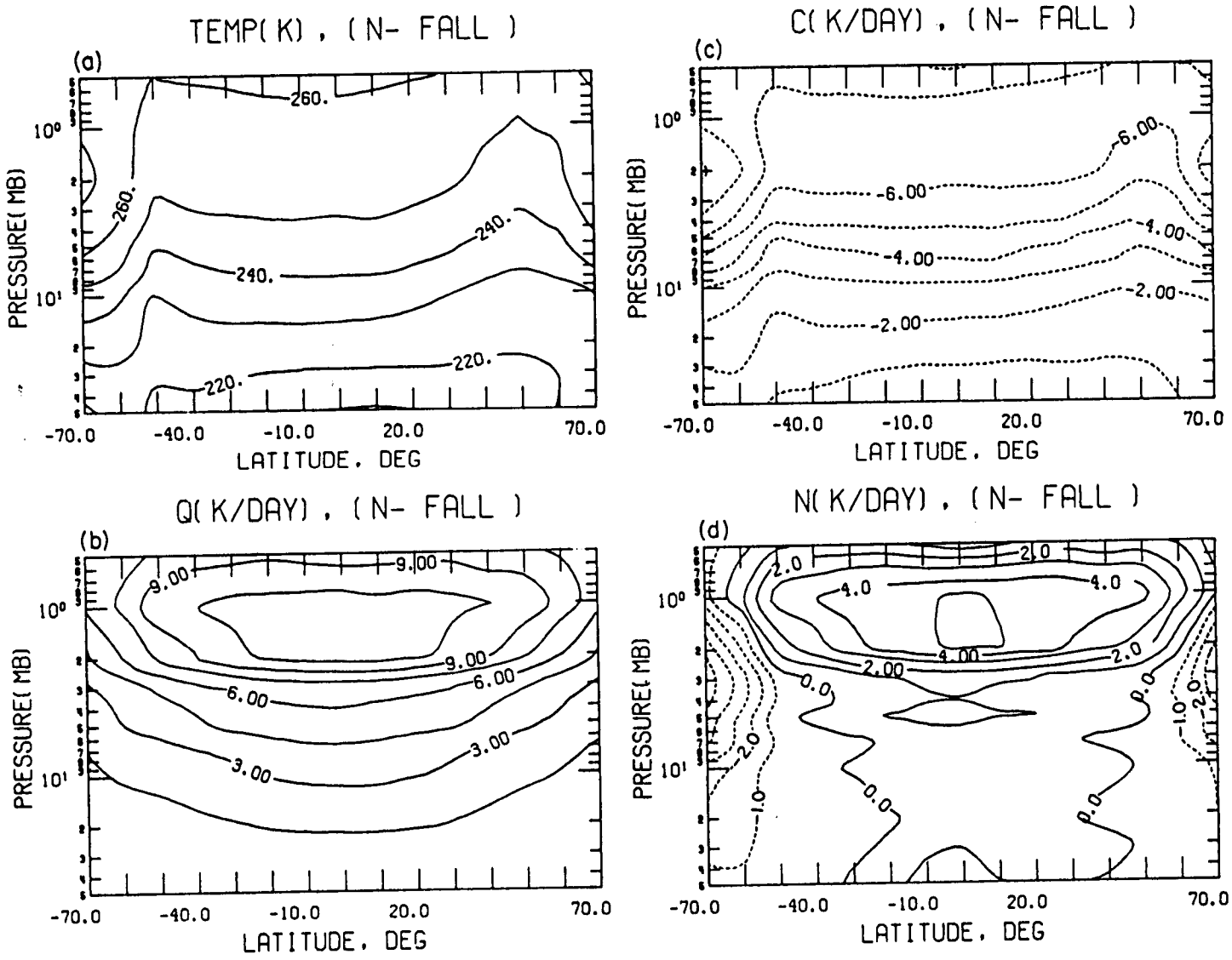
TEMP(K) , (N- FALL)
(a)
260.
260.
240.
240.
220.
220.
PRESSURE(MB)
LATITUDE, DEG
C(K/DAY) , (N- FALL)
(c)
6.00
-6.00
4.00
-4.00
2.00
-2.00
Q(K/DAY) , (N- FALL)
(b)
9.00
6.00
3.00
N(K/DAY) , (N- FALL)
(d)
4.0
2.0
0.0
-1.0
-2.0
-70.0
-40.0
-10.0
20.0
70.0

Figure 7

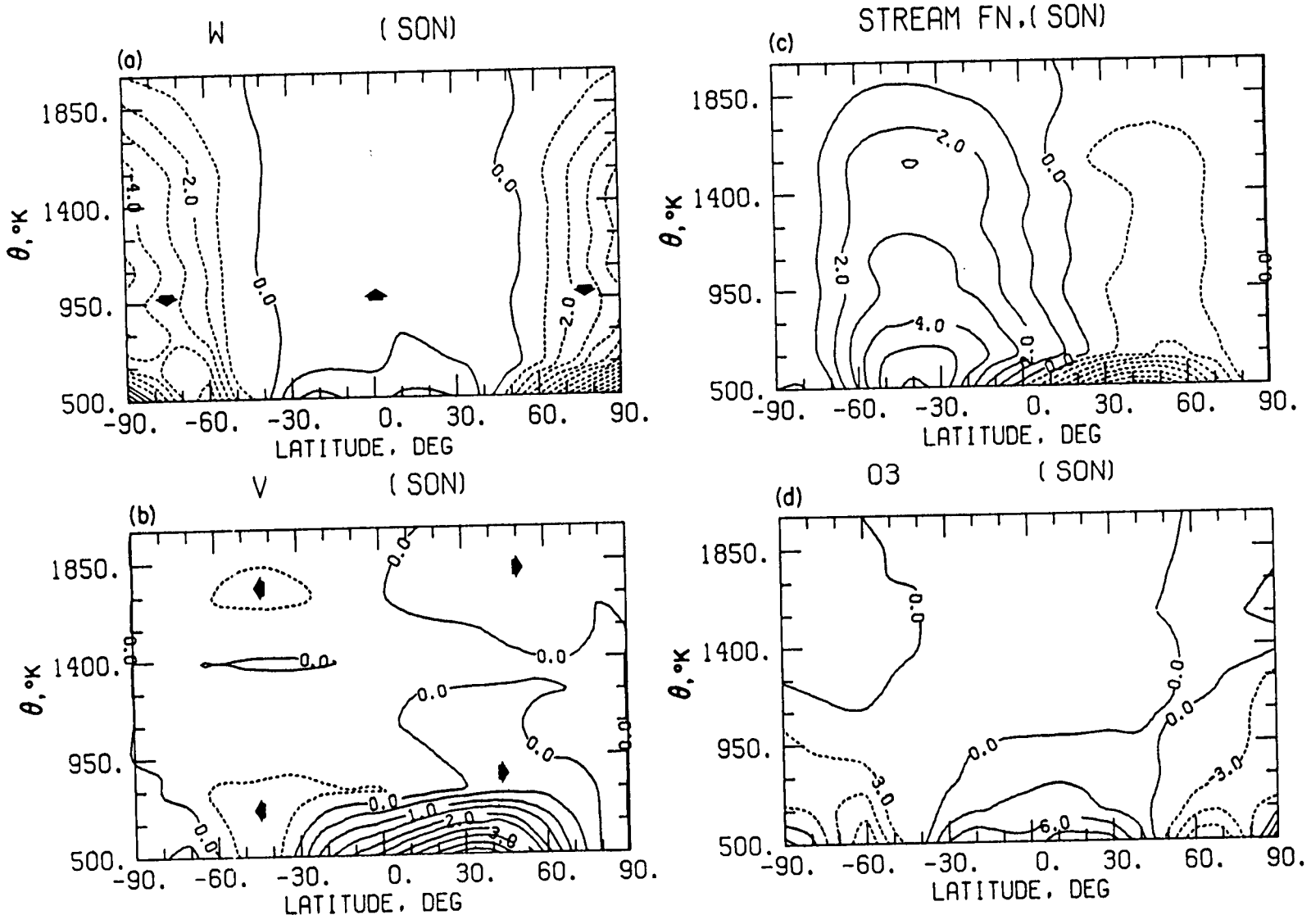
W (SON)
(a)
1850.
1400.
950.
500.
θ, °K
-90. -60. -30. 0. 30. 60. 90.
LATITUDE, DEG
-4.0
-2.0
0.0
2.0
STREAM FN.(SON)
(c)
2.0
0
4.0
V (SON)
(b)
1.0
3.0
O3 (SON)
(d)
6.0

Figure 8

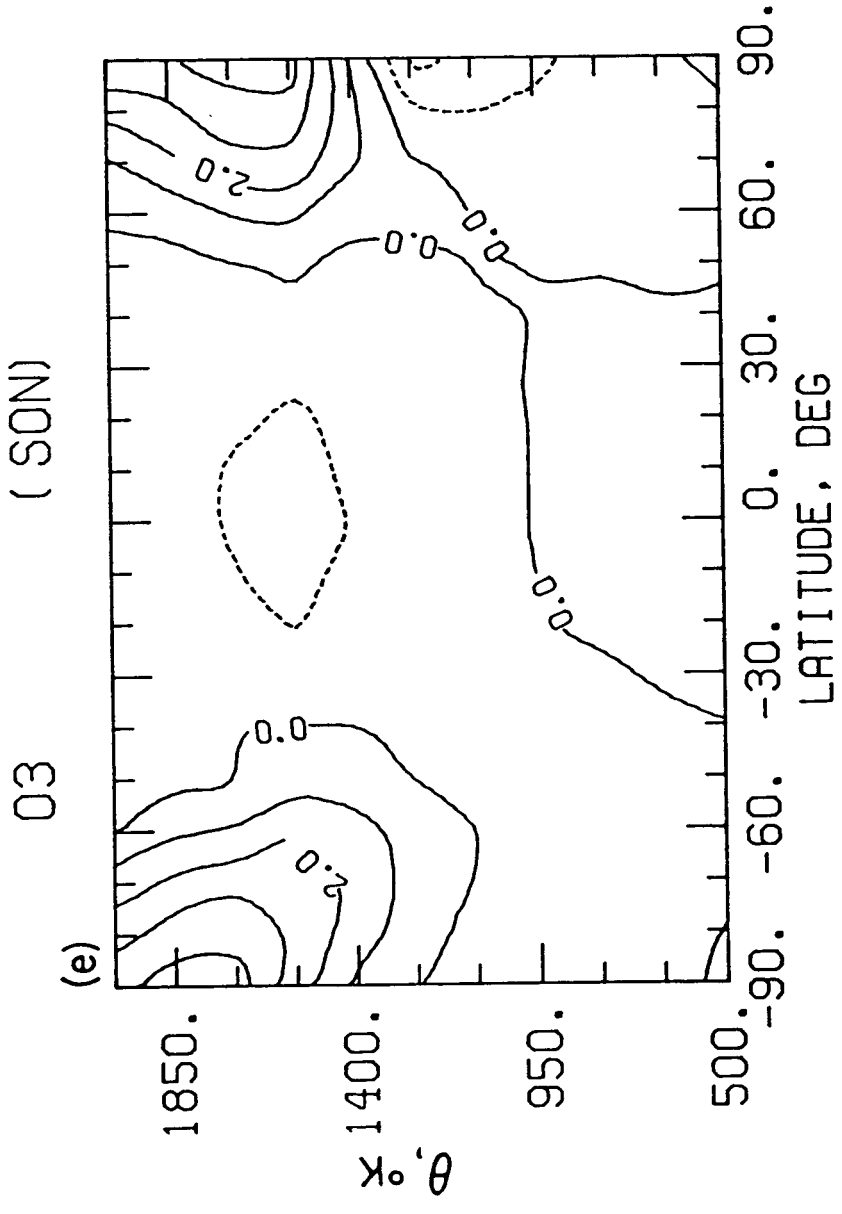
(e)
O3
(SON)
θ, °K
1850.
1400.
950.
500.
-90.
-60.
-30.
0.
30.
60.
90.
LATITUDE, DEG
2.0
0.0
0.0
0.0
0.0
0.0

Figure 8e

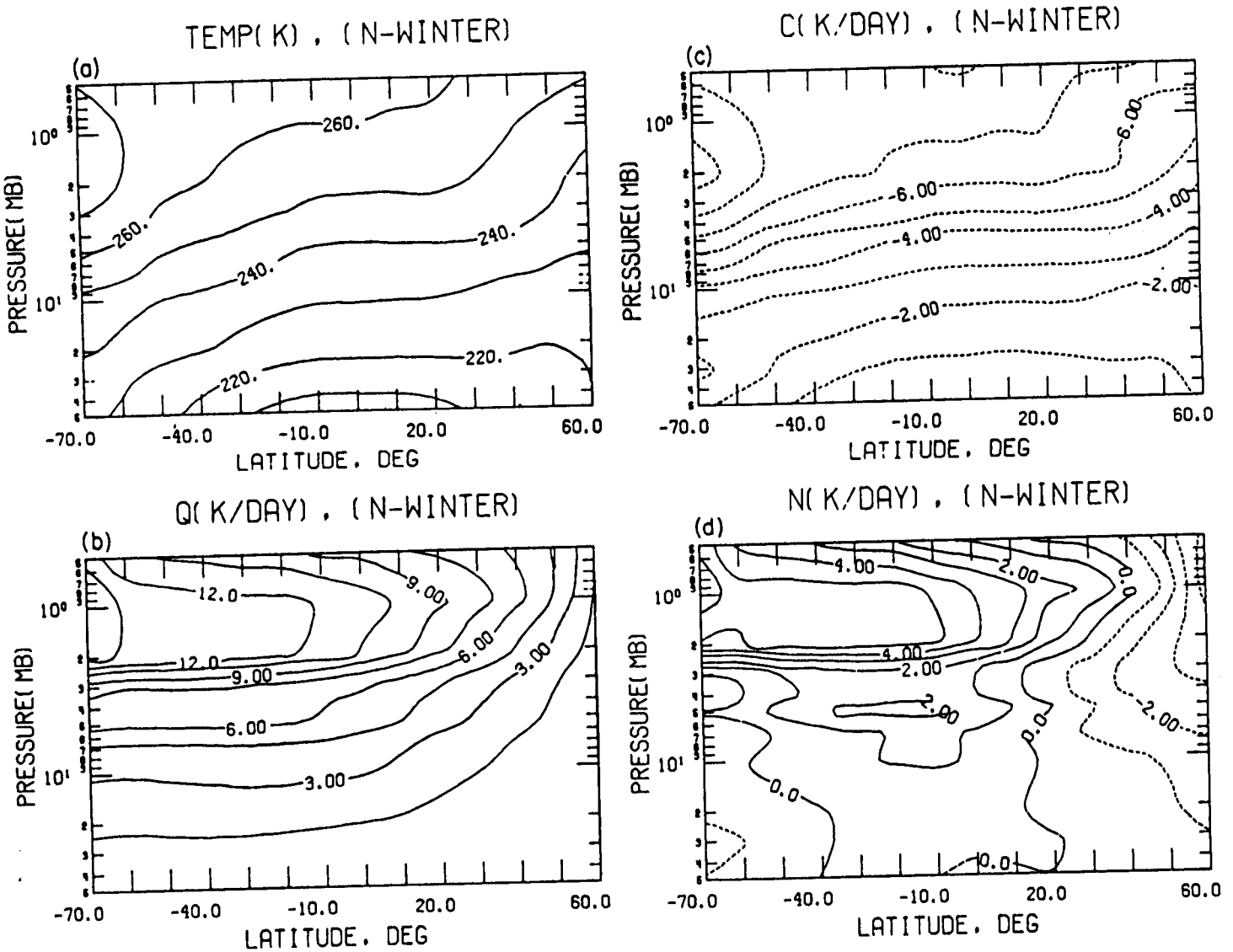
TEMP(K) , (N-WINTER)
(a)
260.
240.
220.
PRESSURE(MB)
LATITUDE, DEG
C(K/DAY) , (N-WINTER)
(c)
6.00
4.00
2.00
Q(K/DAY) , (N-WINTER)
(b)
12.0
9.00
6.00
3.00
N(K/DAY) , (N-WINTER)
(d)
0.0
-70.0
-40.0
-10.0
20.0
60.0

Figure 9

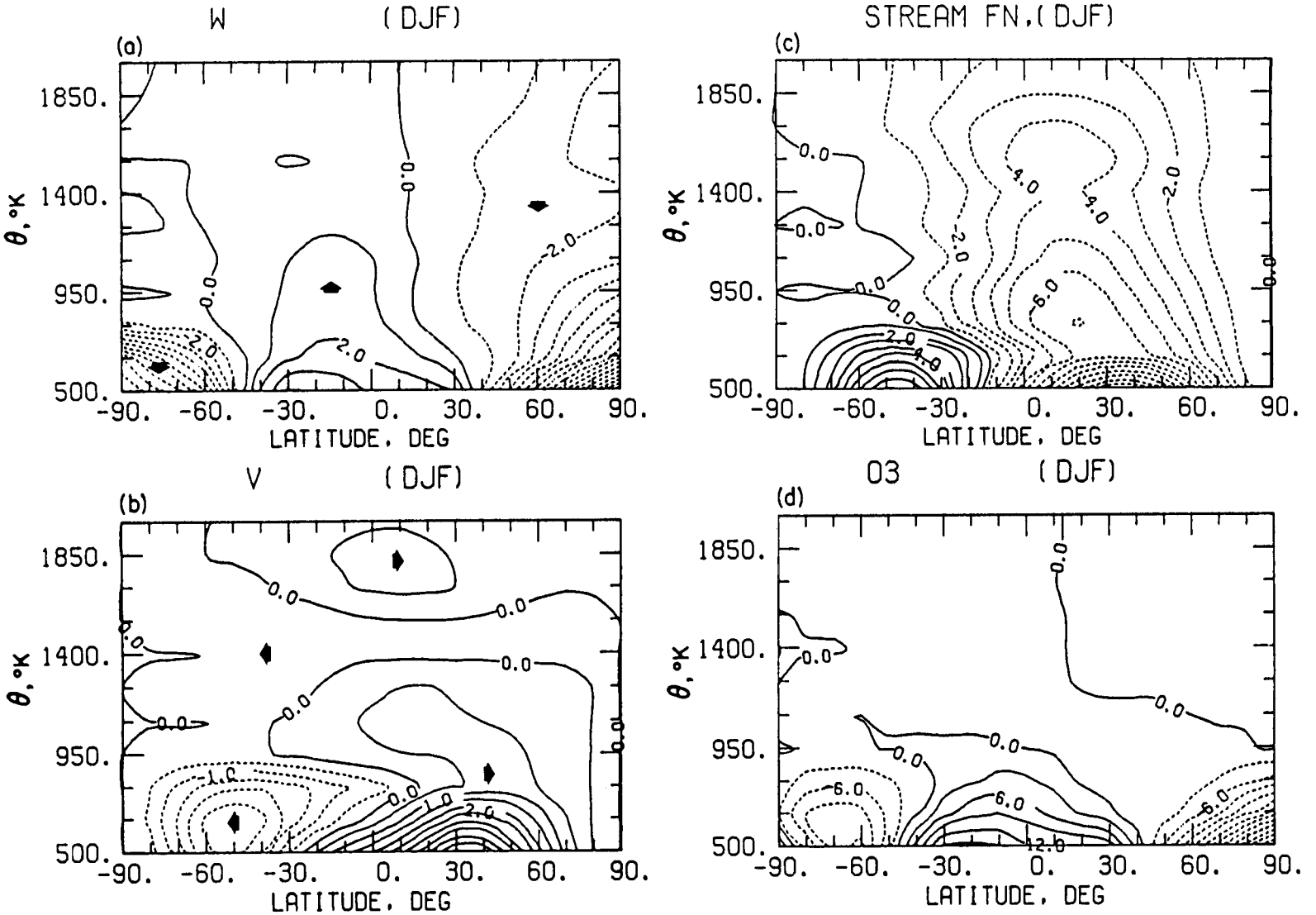
W (DJF)
(a)
STREAM FN.(DJF)
(c)
V (DJF)
(b)
O3 (DJF)
(d)
θ, °K
1850.
1400.
950.
500.
-90. -60. -30. 0. 30. 60. 90.
LATITUDE, DEG

Figure 10

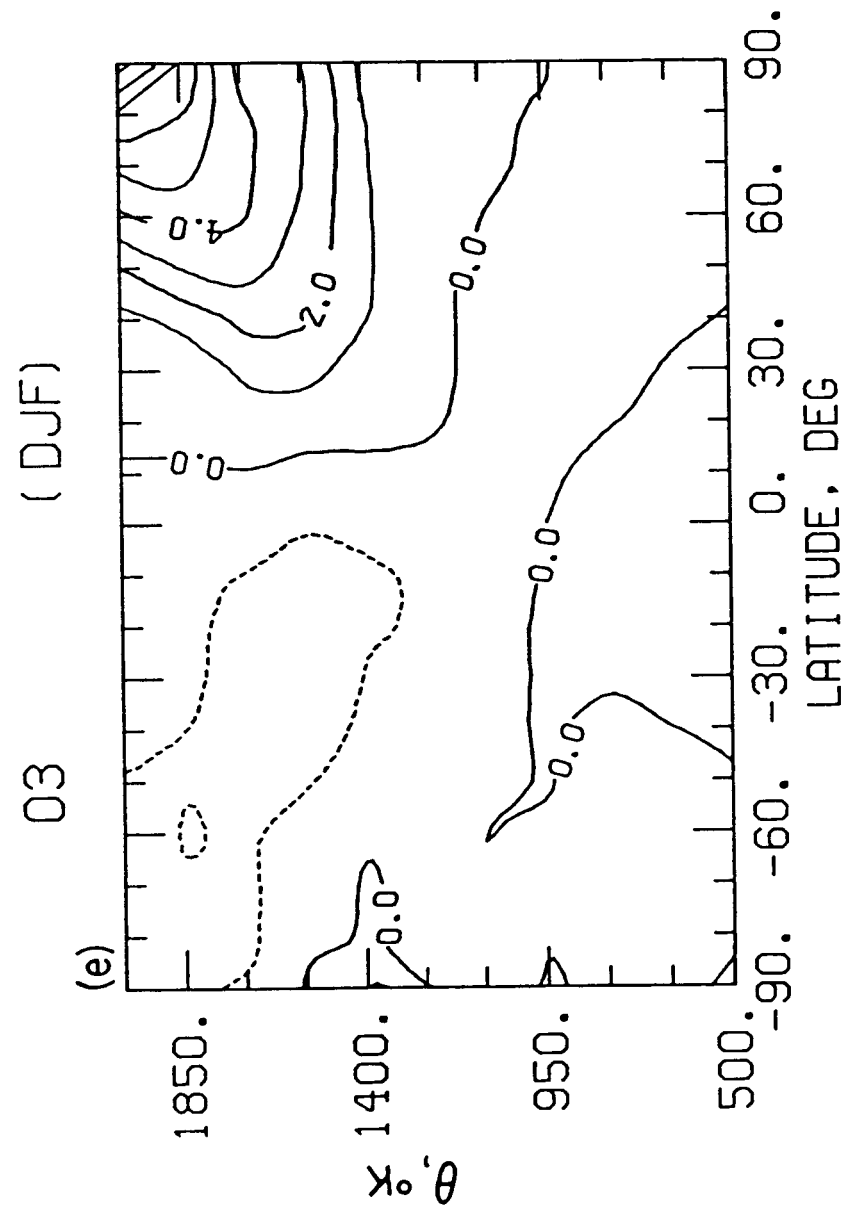
(e)
O3
(DJF)
4.0
2.0
0.0
0.0
0.0
0.0
0.0
1850.
1400.
950.
500.
θ, °K
-90.
-60.
-30.
0.
30.
60.
90.
LATITUDE, DEG

Figure 10e